









RESEARCH ARTICLE | JUNE 06 2023

The real honeycomb structure—From the macroscopic down to the atomic scale

Leonard Gura ; Matthias Brinker ; Patrik Marschalik; Florian Kalaß ; Bettina Junkes ; Heinz Junkes ; Markus Heyde  ; Hans-Joachim Freund 

 Check for updates

Journal of Applied Physics 133, 215305 (2023)

<https://doi.org/10.1063/5.0148421>


View
Online


Export
Citation

CrossMark

AIP Advances

Why Publish With Us?

-  **25 DAYS**
average time to 1st decision
-  **740+ DOWNLOADS**
average per article
-  **INCLUSIVE**
scope

[Learn More](#)

 AIP
Publishing

The real honeycomb structure—From the macroscopic down to the atomic scale



Cite as: J. Appl. Phys. 133, 215305 (2023); doi: 10.1063/5.0148421

Submitted: 1 March 2023 · Accepted: 11 May 2023 ·

Published Online: 6 June 2023



Leonard Cura,¹  Matthias Brinker,¹  Patrik Marschalik,¹ Florian Kalaß,¹  Bettina Junkes,²  Heinz Junkes,¹ 
Markus Heyde,^{1,a)}  and Hans-Joachim Freund¹ 

AFFILIATIONS

¹Fritz-Haber-Institut der Max-Planck-Gesellschaft, Faradayweg 4-6, 14195 Berlin, Germany

²Imkerei Berliner Garten Honig, Lützelsteiner Weg 41, 14195 Berlin, Germany

^{a)}Author to whom correspondence should be addressed: heyde@fhi-berlin.mpg.de

ABSTRACT

The honeycomb's eponymous structure is omnipresent in our every day lives. We want to provide some inspiration to perform structural analyses of these structures and to draw comparisons between them. In the present study, we detect honeycomb patterns and related complex network structures on different length scales ranging from macroscopic objects down to the atomic scale of 2D materials. In 2D materials, a subset of the honeycomb structure—the kagome lattice—is very interesting due to unique material properties. For structure detection, we developed a program written in Python. The program is very adaptable and provides a graphical user interface to modify the detected network interactively. With the help of this program, we directly compare honeycomb structures with atomic network structures. Both honeycombs and 2D atom networks can show local deviations from their characteristic hexagonal pattern. The structural deviations at the macroscopic scale and at the atomic scale are very similar. We provide additional structural analyses of every day objects and encourage everyone to use our software that is freely accessible.

© 2023 Author(s). All article content, except where otherwise noted, is licensed under a Creative Commons Attribution (CC BY) license (<http://creativecommons.org/licenses/by/4.0/>). <https://doi.org/10.1063/5.0148421>

I. INTRODUCTION

Networks and the analysis of their structures are very important in many disciplines ranging from communication over neural networks to structural materials. Basic structural properties have been investigated for a long time.^{1,2} Nature exhibits diverse network arrangements. The most prominent network structure consists of hexagonal patterns. This so-called honeycomb structure is well known and omnipresent in our everyday lives in the form of meaningful logos, as decorative tiles, and in structural elements. This is not only true for macroscopic objects that are visible to the naked eye but also for microscopic systems.

Even atoms arrange in hexagonal lattices, as discussed in introductory textbooks on crystallography.^{3,4} One example of such a material exhibiting a hexagonal atomic lattice is crystalline silicon dioxide (quartz). The non-crystalline phase of SiO₂ is commonly known as glass and has been used by humans for thousands of years. The question how the atoms arrange in this vitreous phase is one of the most fundamental questions in science.⁵

Almost 100 years ago, Zachariassen discussed the atomic arrangement in silicon dioxide with the two-dimensional (2D) model shown in Fig. 1.⁶ The two different phases are shown: the crystalline, hexagonal phase in Fig. 1(a) and the vitreous phase in Fig. 1(b). Both phases consist of the same building block shown at the bottom of Fig. 1. Three anions (oxygen) surround the cation (silicon) in the center resulting in a kagome lattice. For such kagome lattices, theoretical calculations predicated unique materials properties.^{7,8} Recently, these predictions could be verified experimentally.^{9,10}

In the crystalline phase of the 2D silicon dioxide film, the building blocks connect in angles of 120°. The resulting hexagons, also called six-membered rings, form the periodic structure shown in Fig. 1(a). In the vitreous phase, the building blocks arrange in varying angles. This results in different SiO₂ ring sizes. Some rings are formed by only four building blocks, while others consist of five, six, seven, or even more building blocks. The variation in ring sizes results in the non-periodic arrangement shown in Fig. 1(b). This vitreous phase represents the atomic model structure for glass.

As obvious from this model, it is known for a long time that even the most fundamental structures—atomic networks of materials—show hexagonal patterns. More importantly, deviations from the hexagonal structure are expected in systems such as silicon dioxide. Figure 2 provides three examples from the literature where hexagonal atomic networks and their structural deviations have been studied.

A simple elementary network forming material is carbon. Carbon atoms in graphite and its single layer graphene, for instance, arrange in hexagons. Since the discovery of graphene, the hexagonal structure is often related to 2D materials and its outstanding properties.^{11–16} Figure 2(a) shows a theoretical model of graphene in both the crystalline and the vitreous configuration.

To image the atomic structure of 2D materials, advanced microscopy techniques are required that have a spatial resolution below an Ångström (10^{-10} m). A prominent real space technique with extraordinary spatial resolution is scanning tunneling microscopy (STM), which relies on the quantum tunneling effect. The sharp metal tip of the STM scans across the surface while a potential difference is applied between tip and surface. By measuring the resulting tunneling current, atomic sites can be visualized.^{17,18}

The first atomically resolved network that shows both crystalline and vitreous structures is the 2D phase of silicon dioxide, which was discovered 10 years ago.¹⁹ With STM, the hexagonal pattern—which is commonly called honeycomb structure - could be detected down to the atomic scale, as shown in Fig. 2(b). Also, the vitreous phase of the 2D SiO_2 film was revealed with atomic precision. Remarkably, the measurements agree very well with the predictions made almost 100 years ago by Zachariasen.^{6,20}

Since the discovery of the vitreous 2D phase of SiO_2 - the thinnest glass film—the research field of non-periodic films is growing and the structural deviations gain in importance in science and research. For further reading, we refer to the original publications and recent review articles.^{19,23–25}

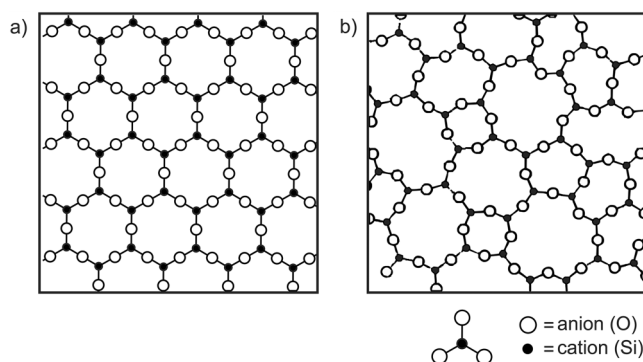


FIG. 1. Theoretical models of the SiO_2 structure. (a) The crystalline honeycomb structure. (b) The non-periodic structure according to the random network model by W.H. Zachariasen.⁶ The unit block is the same for both structures. Anions are drawn as white and cations as black circles, as shown on the bottom. Adapted with permission from Zachariasen, *J. Am. Chem. Soc.* **54**, 3841 (1932). Copyright 1932 American Chemical Society.

Also on larger length scales of several tens of nanometers similar structures with different ring sizes have been observed. Rubrene ($\text{C}_{42}\text{H}_{28}$) molecules, for instance, assemble in supramolecular rings representing pentagons, hexagons, and heptagons. The resulting domains show different densities and degrees of order.²⁶ In another example, STM measurements could reveal that 1,3,5-tris(4-bromophenyl)benzene (TBPB) monomers form nanoporous networks with crystalline and vitreous areas.²² In this case, not the atoms form a network with different ring sizes but the monomers form covalent bonds resulting in either crystalline or vitreous structures. The crystalline monomer network is shown in Fig. 2(c) on the left. The vitreous configuration is shown on the right. The monomer and the resulting nanopores are shown in the center of Fig. 2(c).

As mentioned at the very beginning, hexagonal structures are also present in macroscopic objects, visible to the naked eye. Figure 3 gives three everyday life examples that show both

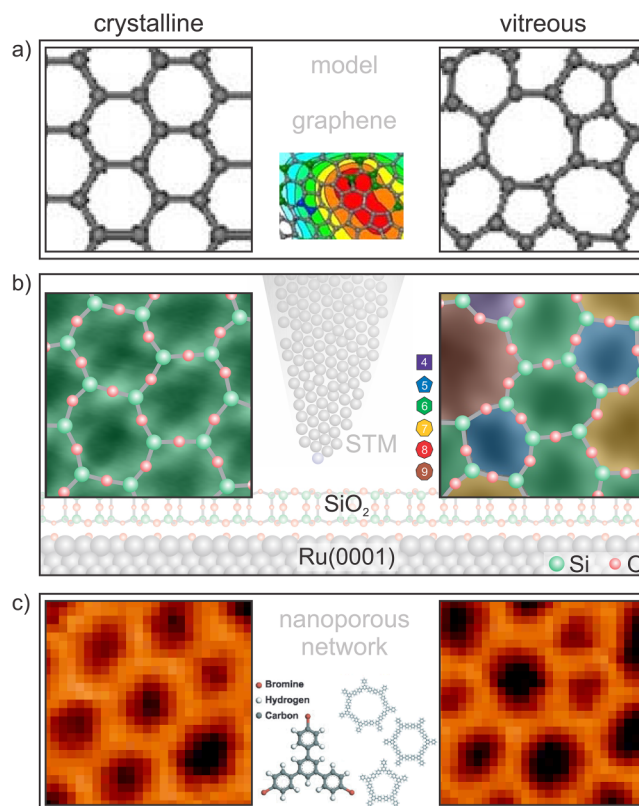


FIG. 2. Atomic network structures. (a) Theoretical model of graphene. Adapted with permission from Li and Drabold, *Phys. Stat. Sol.* (b) **250**, 1012 (2013). Copyright 2013 John Wiley & Sons. (b) STM images of the atomic arrangement of SiO_2 ($1.3 \times 1.3 \text{ nm}^2$). Adapted with permission from Lichtenstein *et al.*, *J. Phys. Chem. C* **116**, 20 426 (2012). Copyright 2012 American Chemical Society. (c) STM images of TBPB ($60 \times 60 \text{ nm}^2$). Adapted with permission from Blunt *et al.*, *Chem. Commun.* **46**, 7157 (2010). Copyright 2010 Royal Society of Chemistry.

crystalline and vitreous patterns. Bubblerfts appear on several liquids. The most common example are soap bubbles in a bathtub. Prepared in a controlled way, Bragg and Nye have used these systems to teach their students about atomic models and to illustrate the arrangement of domain boundaries and the effects of strain.²⁷ A similar approach lead to a simple model system enabling students to study vitreous arrangements, as shown in Fig. 3(b).²⁸

Naturally grown organisms also show hexagonally arranged units, such as the grains of maize in Fig. 3(c). As in many natural growth processes, these periodic patterns can be distorted due to different reasons. An example is shown in Fig. 3(d). The arrangement of the grains obviously shows deviations from the hexagonal

pattern. Another example showing both crystalline and vitreous structures are different types of corals. The extinct tabulate coral (Favosite) in Fig. 3(e) exhibits closely packed corallites resulting in the hexagonal honeycomb structure. The coral in Fig. 3, on the other hand, exhibits a non-periodic arrangement.

The few examples above already demonstrate the broad range of structural configurations on both the atomic and the macroscopic scale. In many disciplines, the structural analysis of these arrangements is of great importance. The unique arrangements ask for new analysis tools and characterization methods. We present custom programmed software that enables the interactive analysis of non-periodic structures. With this software, we want to provide the basic analysis tools for students, researchers, and curious observers, in general, to enable them to study non-periodic structures on different length scales.

In the present study, we compare hexagonal structures and deviations from this ordered pattern on different length scales ranging from macroscopic objects down to atoms. We focus on honeycombs and atomic networks structures and thereby provide examples how to compare structures on different length scales.

The term “honeycomb structure” is widespread to describe hexagonal patterns in everyday life, arts, and technology. Remarkably, the origin and the function of the hexagonal pattern in honeycombs is still debated.^{31–34} Bees either create these structures by pure instinct, as already pointed out by Darwin more than 150 years ago³⁵ or with a certain intelligence, as proposed by Wyman a few years later.³⁶ The question arises whether bees deviate from this habit and whether there are exceptions from the regular pattern.

Here, we want to allow students and researchers to interactively work with diverse structural arrangements. By characterizing structural patterns in detail, rules and common features can be identified that were not obvious at first sight. To visualize and to analyze these structures, we developed purely Python³⁷ based software, named *visualyse*. The software provides semi-automated network detection algorithms and graphical user interfaces (GUIs) to enable interactive adjustments of the networks. In the following sections, we introduce the program that is freely accessible.³⁸ In the supplementary material, we provide videos that serve as basic Instructions on how to use the program. We developed the program with the purpose to provide a user friendly network creation tool. The network serves than as basis for detailed and thorough structural analysis. Compared to studies that have been performed since the early 18th century,³⁹ these tools facilitate faster and more diverse structural analysis.

With the help of the semi-automated network detection software, we want to answer the question: Can we detect deviations from the hexagonal structure in honeycombs and how do these deviations compare to honeycomb-like atomic networks of 2D glass films?

II. EXPERIMENTAL DETAILS

Honeycombs consist of beeswax (*cera alba*), which is naturally produced by honey bees. Figure 4 shows two examples of honeycombs grown by Western honey bees (*Apis mellifera*).⁴⁰ The photograph in Fig. 4(a) shows the bees on a naturally grown honeycomb.

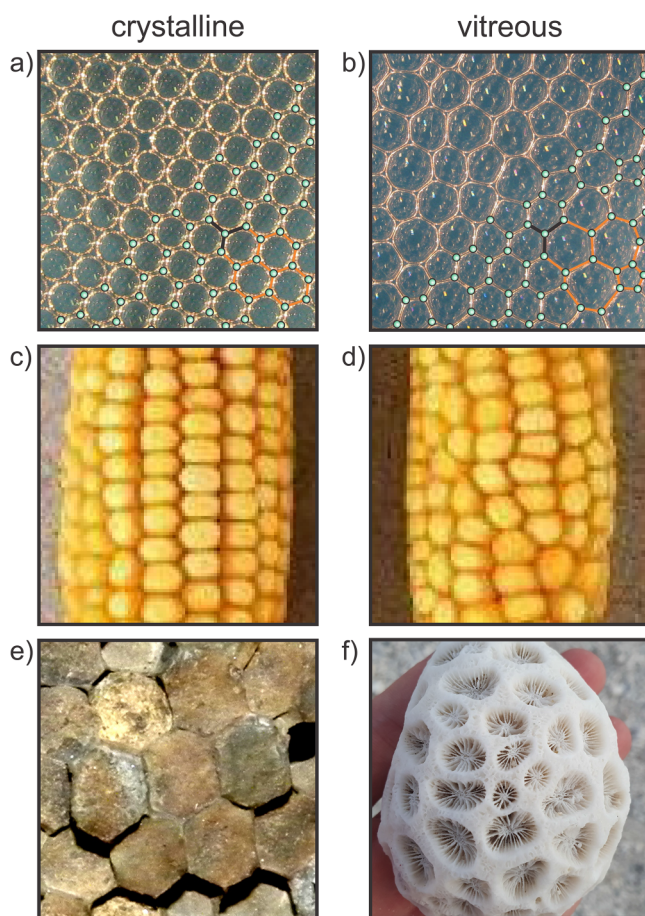


FIG. 3. Macroscopic objects with hexagonal structures. (a) and (b) Bubblerfts with crystalline and vitreous arrangements.²⁸ Adapted from Burson *et al.*, *J. Chem. Educ.*, **92**, 1896 (2015); licensed under a Creative Commons Attribution (CC BY) license. The connection points are marked in green. The basic unit block is the same for both cases similar to Fig. 1. Different bubble sizes are highlighted with orange lines. (c) and (d) Corn ($7 \times 7 \text{ cm}^2$).²⁹ Adapted with permission from Peter Thomison. (e) and (f) Corals. (e) Favosite, also called “honeycomb coral” ($1.1 \times 1.1 \text{ cm}^2$).³⁰ Adapted with permission from Wilson. (f) Coral with a vitreous network ($7.5 \times 7.5 \text{ cm}^2$).

The honeycomb is fixed in a wooden frame. No additional support is provided to construct the honeycombs. The photograph in Fig. 4(b) on the other hand shows honeycombs grown on a flat pre-defined wax grid. The wax grid serves as a starting point for the bees and consists of the same natural wax as the honeycombs. To build the honeycombs, wax from this grid can be used and modified.

Both honeycombs in Fig. 4 are very bright in color indicating that these combs have not been used as brood combs but served for honey storage only. The combs are imaged after the honey season and will be used again as honey storage in following seasons.

To avoid image distortions as present in the photograph in Fig. 4(b), we scanned the honeycombs with a commercial flat bed scanner of the CX series from Lexmark. Figure 5(a) shows a characteristic segment of such a scan with the wooden frame on the left and the right edges.

Images of atomic structures are taken from published work. In the present study, we show images acquired with scanning tunneling microscopy (STM)^{25,41–43} and atomic force microscopy (AFM).⁴⁴

Both atomic scale images and scans of macroscopic honeycombs are analyzed with the semi-automated network detection software. The software is purely Python³⁷ based, can be installed on any operation system and is freely accessible.³⁸ Scan files and images can be loaded into the GUI as illustrated in the supplementary material. To accelerate subsequent analyses, images can be downscaled in advance.

For illustration, the honeycomb structure in the highlighted section in Fig. 5(a) is analyzed. Figure 5 illustrates the process of network detection. First, the centers of the polygons are detected. The centers correspond to intensity minima, i.e., dark areas in the image. To detect only the centers and not all local intensity minima, the image is slightly blurred with a Gaussian filter. The result of the center detection is shown in Fig. 5(b). The mouse cursor indicates that the detected center position can be modified interactively in the graphical user interface of the Python program, which is created with the visualization toolkit (vtk).⁴⁵

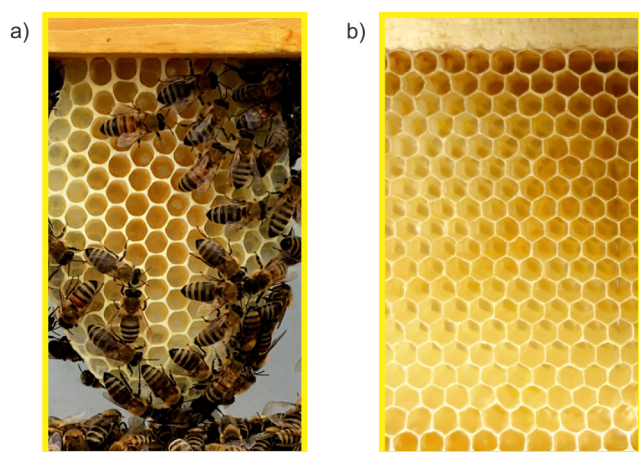


FIG. 4. Photographs of honeycombs. (a) Honeycomb without and (b) with supporting wax grid ($6 \times 10 \text{ cm}^2$).

In the following step, the neighborhood of every polygon is detected with a random walker algorithm to segment the image.⁴⁶ For segmentation, the center positions serve as starting points. Neighboring segments are then connected as indicated by straight gray lines in Fig. 5(c). The connectivity, i.e., the straight lines can be adjusted interactively by the user. The representation with points and lines is the graphical illustration of a mathematical graph. In the described case of connecting neighbored segments, a region adjacency graph (RAG) is generated. The advantage of the mathematical graph is that it allows to analyze the detected network extensively with little time and effort.

To mimic the polygons in the image, the program calculates the network based on geometrical considerations. The central point of three connected center positions (nodes of the RAG) is connected. The result is another mathematical graph whose graphical illustration corresponds to the network drawn in white in Fig. 5(d). The detected polygons are color coded in Fig. 5(e). Hexagons are assigned to the color green.

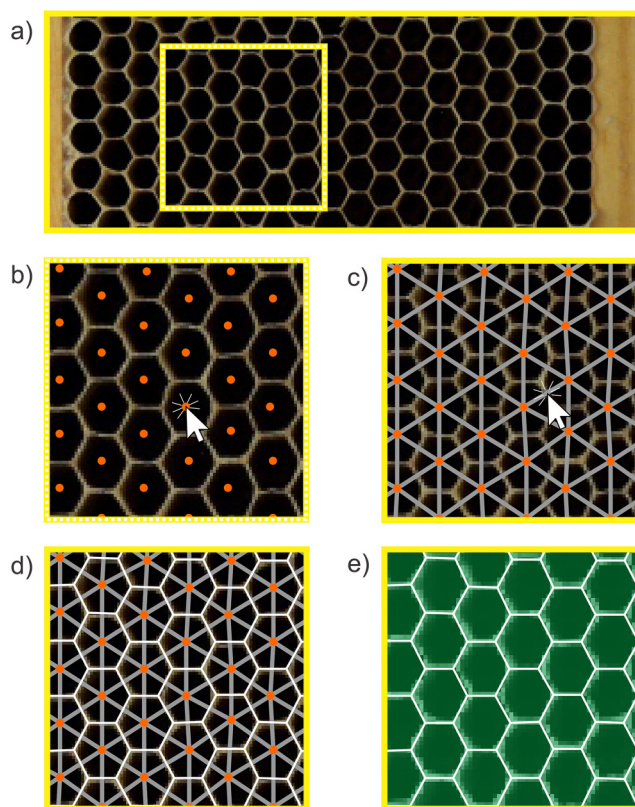


FIG. 5. Semi-automated detection of the honeycomb structures. (a) Honeycomb scanned with a Lexmark flat bed scanner ($10.1 \times 3.7 \text{ cm}^2$). (b) Identification of polygon centers. (c) Detection of neighbored polygons. (d) Construction of the network based on geometric considerations. (e) Color coding of polygons for visualization ($2.7 \times 2.7 \text{ cm}^2$).

While projects treating the topic of segmentation exist already,⁴⁷ the embedding in an interactive graphical user interface and the building of networks that resemble structural arrangements has not been done so far to the best of our knowledge. Our step toward the reconstruction of atom network models based on this kind of image analysis is promising for many imaging techniques in the field of chemistry and physics.

III. RESULTS AND DISCUSSION

We applied the semi-automated network detection to a selection of representative atomic “honeycomb structures” to compare them to the eponymous macroscopic honeycomb structure. Figure 6(a) shows the hexagonal structure of the macroscopic honeycomb that was detected in Fig. 5. All macroscopic honeycombs in this publication are shown in yellow frames. The hexagons are drawn in white and are color coded in green. To compare this macroscopic structure to atomic structures of representative materials, we applied the semi-automated network detection to scanning probe microscopy images from the literature of graphite, mica, and 2D silica. All images of 2D silica in this publication are shown in gray frames. Figures 6(a)–6(c) show that only hexagons are detected in these image sections. In this direct comparison, the similarity between the periodic hexagonal structures of the

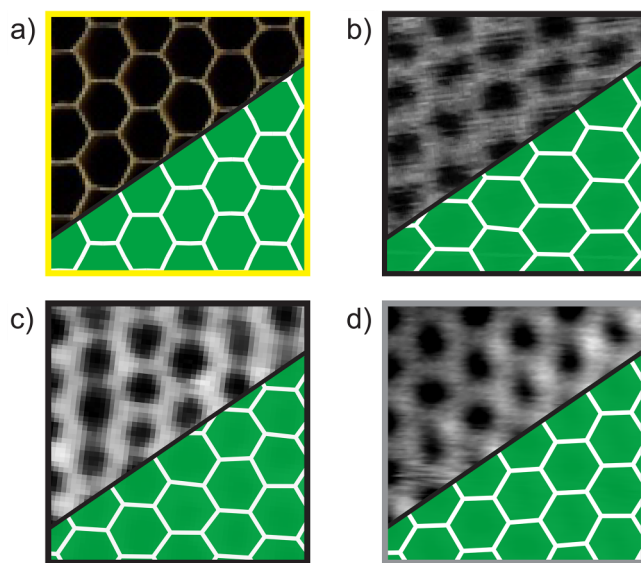


FIG. 6. Hexagonal patterns of Bee honeycombs in comparison to atomic scale surface structures. (a) honeycombs ($2.7 \times 2.7 \text{ cm}^2$). (b) graphite (STM, $1.1 \times 1.1 \text{ nm}^2$). Adapted with permission from Atamny *et al.*, Phys. Chem. Chem. Phys. **1**, 4113 (1999). Copyright 1999 Royal Society of Chemistry. (c) Cleaved (001) surface of muscovite mica (FM-AFM, $2.7 \times 2.7 \text{ nm}^2$). Reproduced from Fukuma *et al.*, Appl. Phys. Lett. **87**, 034101 (2005). Copyright 2005 AIP Publishing LLC. (d) The 2D silica film (STM, $2.7 \times 2.7 \text{ nm}^2$). Reproduced with permission from Burson *et al.*, J. Phys. Condens. Matter **29**, 035002 (2017). Copyright 2017 IOP Publishing Ltd. Bee honeycombs are highlighted with yellow frames and 2D silica films are highlighted with gray frames.

macroscopic honeycombs and the atomic structures at the nanometer scale becomes obvious.

Not without reason these atomic arrangements are often referred to as “honeycomb structure.” To answer the question how the structural properties of these two systems that bridge length scales of exactly seven orders of magnitude compare to each other, Fig. 7 shows the color coded center–center distances. The average center–center distance of the macroscopic honeycomb structure in Fig. 7(a) is 0.54 cm. For the silica film in Fig. 7(b), the average center–center distance is 0.53 nm. The color code range of all distance plots is set to these average distances $\pm 50\%$.

The distances do not show large deviations in these crystalline sections. However, in the upper right corner of the silica film in Fig. 7(b) marked with a dashed rectangle, the deviations are larger. Considering the neighborhood of this section shown in Fig. 7(c), it becomes obvious that the adjacent rings are not hexagons. As mentioned above, the structure of 2D silica films can exhibit deviations from the hexagonal pattern. In the case of Fig. 7(c), five- to eight-membered rings are detected, represented as pentagons, hexagons, heptagons, and octagons. In the vicinity of these structural deviations, the color coded center–center distances show broader distributions. Considering these deviations from the hexagonal pattern, is it wrong to name the 2D silica film “honeycomb structure”?

We carefully checked several honeycombs and detected regions that show deviations from the familiar hexagonal pattern. Figure 8(a) shows an example of such honeycomb structures that

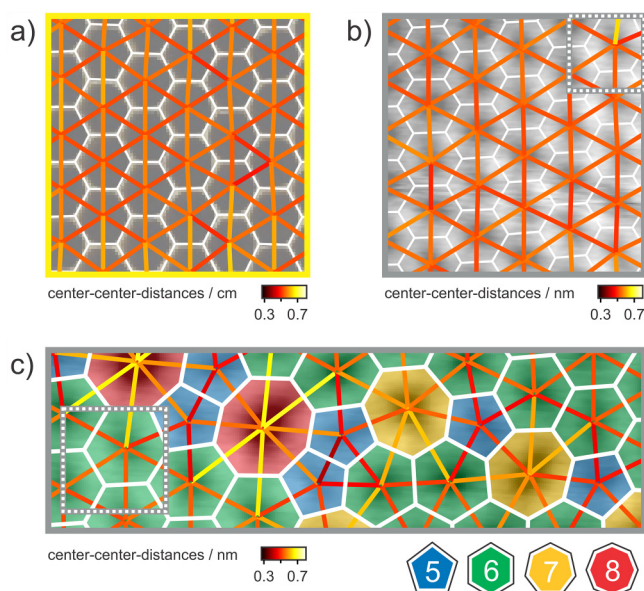


FIG. 7. Center–center distances of crystalline honeycombs in (a) and 2D silica (b). Bee honeycombs are highlighted with yellow frames and 2D silica films are highlighted with gray frames. (c) shows structural deviations in 2D silica in the adjacent region of (b). (a) Flat bed scan of honeycombs ($2.7 \times 2.7 \text{ cm}^2$) from (a). (b) STM image of 2D silica ($2.7 \times 2.7 \text{ nm}^2$) from (d). (c) STM image of 2D silica ($4.5 \times 1.4 \text{ nm}^2$). The color code for the drawn polygons is provided at the bottom. The dashed rectangles in (b) and (c) mark the same region.

deviate from the hexagonal periodicity. For direct comparison, Fig. 8(b) shows the glassy 2D silica film.

Without the network analysis, the comparison is not straightforward. Therefore, the network detection program is applied. Figures 8(c) and 8(d) show the color coded polygon formations of the honeycomb and the 2D silica film. With the detected network, we can compare the deviations in macroscopic honeycombs and atomic networks. In the honeycomb, the deviations consist of combinations of pentagons and heptagons. The yellow heptagons build a row-like arrangement with neighboring pentagons. In the atomic network in Fig. 8(d), also three adjacent heptagons are detected that link to pentagons. Locally, the formation is similar to the macroscopic picture in Fig. 8(c). The formations show great similarity

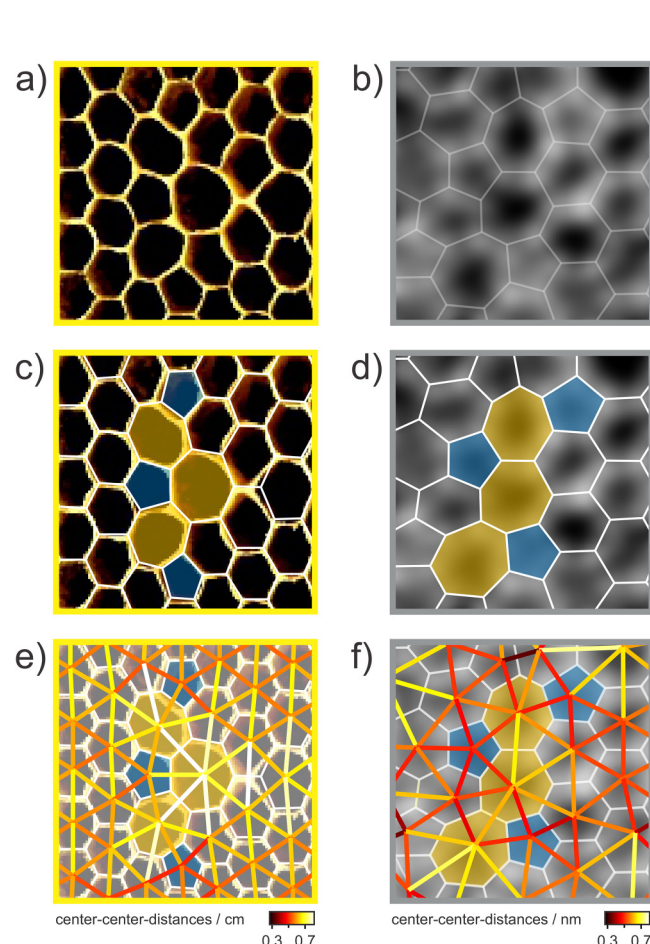


FIG. 8. Deviations from the hexagonal pattern in (a), (c), and (e) honeycombs and (b), (d), and (f) the 2D silica film. Bee honeycombs are highlighted with yellow frames and 2D silica films are highlighted with gray frames. (a) Flat bed scan of honeycombs ($3.2 \times 3.2 \text{ cm}^2$). (b) STM image of 2D silica ($2.3 \times 2.3 \text{ nm}^2$). Adapted with permission from Lewandowski *et al.*, Chemistry 27, 1870 (2021). Copyright 2021 Wiley-VCH GmbH. Honeycombs and 2D silica are overlaid with detected polygons and center-center distances in (c) and (e) and (e) and (f), respectively. Polygons of different sizes are color coded according to the color code in (c).

with the configuration described by Stone and Wales in soccer-ball like fullerenes (C_{60} molecules) consisting of two pentagons and two hexagons.⁴⁸ Furthermore, the formations are similar to the so-called Stone–Wales defect in planar 2D materials that consists of a combination of two pentagons and two heptagons.⁴⁹

The center-center distances of the honeycomb in Fig. 8(e) show that the deviations are largest in the defect region. The distances increase for heptagons and decrease slightly for pentagons. In addition, distances close to these polygon formations deviate considerably. For instance, the vertical connection between the two adjacent hexagons on the right of the defect formation shows an

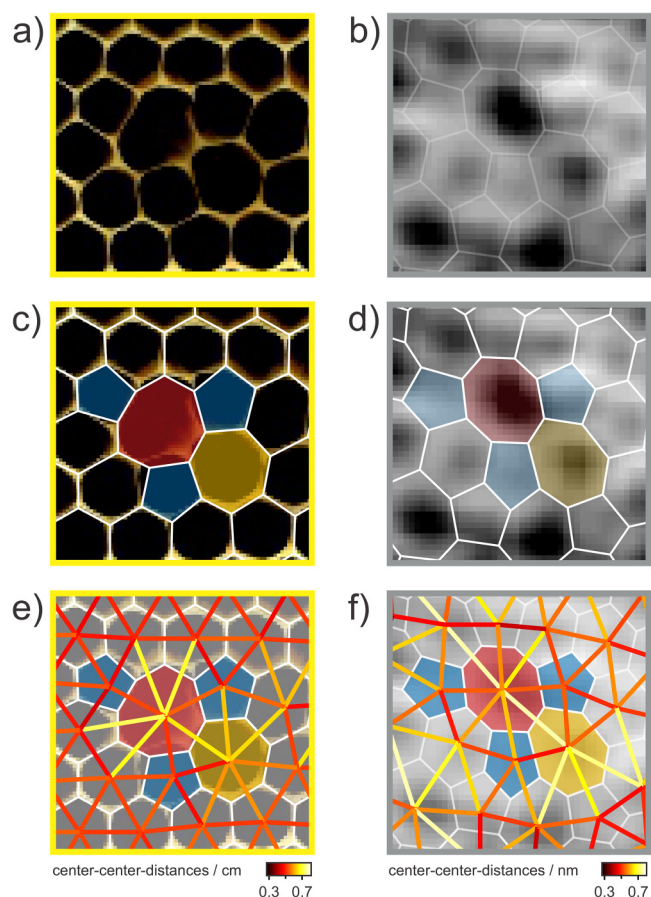


FIG. 9. Deviations from the hexagonal pattern in (a), (c), and (e) honeycombs and (b), (d), and (f) the 2D silica film. Bee honeycombs are highlighted with yellow frames and 2D silica films are highlighted with gray frames. (a) Flat bed scan of honeycombs ($2.2 \times 2.2 \text{ cm}^2$). (b) STM image of 2D silica ($2.3 \times 2.3 \text{ nm}^2$). Adapted with permission from Burson *et al.*, J. Phys. Chem. C 126, 3736 (2022); licensed under a Creative Commons Attribution (CC BY) license. Honeycombs and 2D silica are overlaid with detected polygons and center-center distances in (c) and (e) and (e) and (f), respectively. Polygons of different sizes are color coded according to the color code in Fig. 7(c). Deviations from the hexagonal pattern in (a) and (c) honeycombs, and (b) and (d) the 2D silica film. Polygons of different sizes are color coded.

increased length compared to other center–center distances. In general, the center–center distances in this local section are increased by 5–10% compared to the average distance, as shown in Fig. 7(a). In analogy, the 2D silica film in Fig. 8(f) exhibits increased center–center distances in the defect region for larger rings and shorter distances for smaller rings. In contrast to the defect formation in the honeycomb, the neighborhood in Fig. 8(f) is not fully crystalline but shows minor deviations. These deviations affect the center–center distances in the vicinity of the highlighted defect formation. Still, the analogy between the macroscopic honeycomb and the atomic 2D silica structure can be drawn: center–center distances increase for larger polygons and decrease for smaller polygons.

This observation is remarkable considering that at the atomic scale other constraints apply than in the macroscopic world. For instance, the atom–atom distance and the angles of atomic bonds are rather fixed quantities. On the other hand, bees are not limited by these constraints. Variations in the dimensions of individual honeycombs have been studied for centuries.^{35,36,39} We also observed hexagonal honeycomb formations that show a broad distribution of ring–ring distances, as for instance in Fig. 4(a). More examples are provided in the supplementary material. The largest deviations are observed close to the wooden frame. However, the analyzed defect structures fulfill the above mentioned constraints surprisingly accurately, as shown in Fig. 8(a). The chosen defect formations seem to be energetically favorable at the atomic scale and mechanically stable at the macroscopic scale. In both cases, the defect formation serves as local stress compensation.

Another example in Fig. 9 affirms these observations.

In the honeycomb and the 2D silica film, defect formations of one octagon with one adjacent heptagon and three adjacent pentagons are detected. Figure 9(e) shows that the center–center distances deviate in the defect region. Especially the connecting lines to the large octagon are longer compared to the crystalline average. Similar as the 2D silica in Fig. 8, the structural deviation in the silica film in Fig. 9 is not embedded in a perfect crystalline environment. For this reason, the color coded center–center distances of defect region in Fig. 9(f) are not as pronounced as in Fig. 9(e). Nevertheless increased distances are detected, especially for the connection between the larger ring formation (between the octagon and the heptagon).

As mentioned above, the 2D silica film exhibits larger regions of structural deviations from the crystalline order. Such domains with little to no long range order are called amorphous, vitreous, or glassy. The structure of the glassy 2D silica film has been studied extensively and it was found that it obeys certain rules, such as Euler's theorem. Euler's theorem states that closed planar 2D structures fulfill the following condition, where n is the number of corners of the polygon and k_n is the number of polygons with n corners,

$$\sum_{n=4}^8 (6 - n)k_n = 0. \quad (1)$$

The question arises whether the structural deviations that we observed at the macroscopic scale in the honeycomb structures also

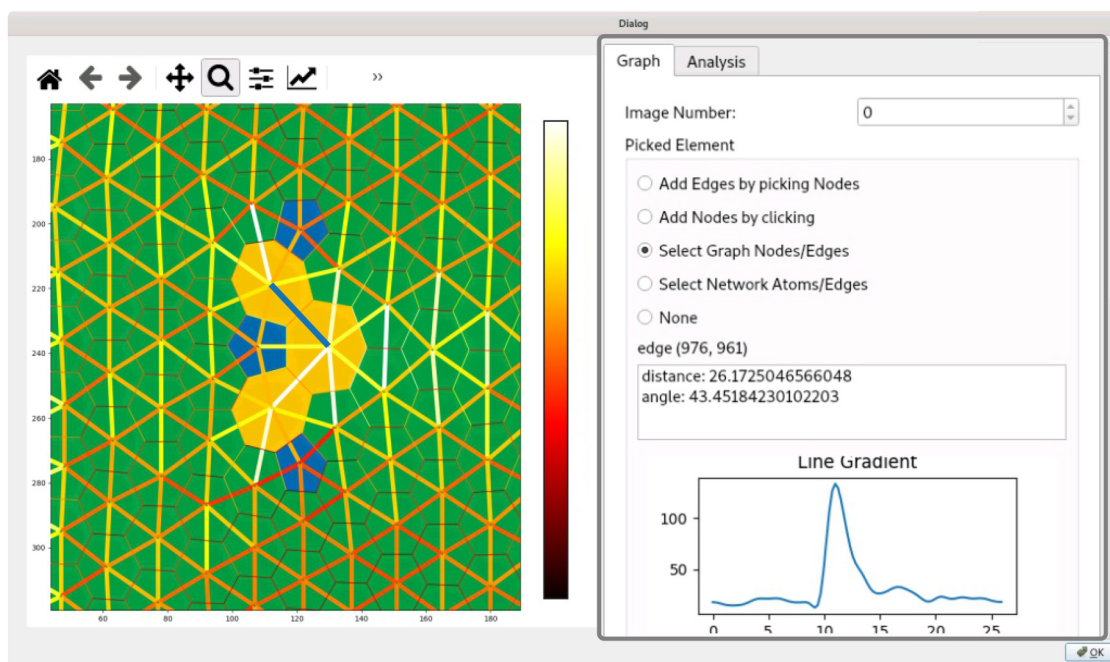


FIG. 10. Edited exemplary screenshot of the graphical user interface of the Python network detection program. On the left, the detected network is shown that can be interactively changed. The visual appearance is fully customizable. The implemented network analysis tools for distances and angles are shown exemplary on the right.

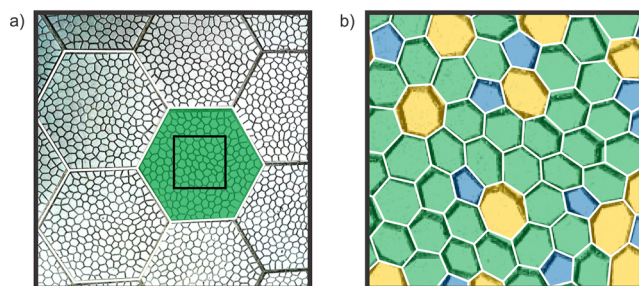


FIG. 11. Hexagonal floor tiles with deviations from the hexagonal pattern within the tile design. (a) Smartphone photograph $40 \times 40 \text{ cm}^2$. (b) Zoomed in section of the photo in (a) of a single tile $7.5 \times 7.5 \text{ cm}^2$. The floor tiles are found at the Fritz-Haber-Institute at Hittorfstraße 29, 14195 Berlin.

fulfill Euler's theorem. In the examples of Fig. 8(c), we detected three pentagons ($n = 5$) and three heptagons ($n = 7$). Thus, the sum in Eq. (1) yields 0 for the honeycomb structure and Euler's theorem is fulfilled. In the case of Fig. 9(c), the sum of one octagon, one heptagon, and three pentagons again yields a value of 0. For these given examples, Euler's theorem is fulfilled in the honeycomb structures. Similar analyses have been performed on the structure of macroscopic bubble rafts.²⁸

In the supplementary material, we show that the bubble rafts can also be analyzed with our network detection software. Due to the optical reflections in the photograph, the automated detection is hindered. Nevertheless, with manual adjustments, the network can be easily drawn. In fact, the network can be generated by solely manual input, as shown on the example of a honeycomb in the supplementary material. Both the manual and automatic detection generate mathematical graphs. The generated mathematical graphs can then be used for detailed structural analysis.

In the software, more analysis tools are incorporated to compare different structural features. Figure 10 provides an edited exemplary screenshot of the graphical user interface. On the left, the detected network of the honeycomb in Fig. 8 is shown.

The network itself and its visual appearance can be modified by the user. The vtk-interface allows to select individual network components, such as nodes and edges. In the case of selected edges, the intensity line profile is plotted automatically and the distances (in pixels) are displayed automatically. For later structural analysis, the network can be color coded with, e.g., the distance or the angle information. The distance distribution can then be scaled to real space coordinates, such as centimeters or nanometers as in Figs. 5, 8, and 9.

The resulting RAG and the network can be exported within the user interface as python networkx graphs⁵⁰ that allow further detailed analysis of, e.g., characteristic distances.⁵¹

As mentioned above, hexagonal structures are widely used and are present in our every day lives. In the last part of the present study, we apply the network detection to an object of our everyday life with no need for high tech microscopes or flat bed scanners. Figure 11 shows a photo of tiles that are recorded with a standard smartphone (Huawei P8 lite) camera. With proper rescaling of the

image dimensions in terms of pixels, our Python software can easily cope with any image file format and enables the quick analysis of the observed structures. Additional examples where we applied the software to everyday life hexagonal structures and their deviations are provided in the supplementary material.

The tiles in Fig. 11(a) exhibit hexagonal shapes, which are outlined in white. The area of a single tile is marked with a black square. Analyzing the pattern of this area, the network in Fig. 11(b) results. Combinations of pentagons and heptagons are present, which shows that the tiles itself incorporate many deviations from the hexagonal pattern.

We found that in many cases, especially in naturally grown hexagonal structures, a closer look reveals deviations from the periodic hexagonal pattern.

IV. CONCLUSION

Honeycombs, their formation, and their structural properties have been studied for centuries and reveal important insights to date. The famous “honeycomb structure” can be found in everyday life and nature exhibits the hexagonal pattern down to the atomic scale. In this study, we detected similarities beyond the periodic hexagonal order between macroscopic honeycombs and atomic networks. Deviations from the “honeycomb structure” appear naturally and show similar characteristics on the centimeter scale and the subnanometer scale. Center-center distances increase for larger polygons and decrease for smaller polygon formations. The defect formations show similar polygon arrangements and fulfill Euler's theorem.

Remarkably, nature does not only exhibit regular structures at the atomic and the macroscopic scale. Nature also builds similar structural deviations on different length scale ranging over more than seven orders of magnitude.

We illustrated that the software tool that we developed is capable of detecting these structural deviations on different length scales independent of how the input image was acquired. The software facilitates the comparison of different networks. To enable easy network detection of arbitrary objects to everyone, the software is freely accessible.

With the shown structure examples, we want to encourage students and researchers to perform structural analysis and use the created mathematical graphs to develop new approaches to characterize non-periodic arrangements. With the presented program, this mathematical graph that forms the basis for this analysis can be easily created.

In future studies, we will focus on structural changes as a function of time. Recently, studies on colloidal graphene on longer timescales are reported.¹⁶ Our developed tools enable such experimental results. The fast network detection allows to study many consecutive images opening the possibility to investigate even faster dynamics on shorter timescales. With our high-speed STM, we can generate such image sequences at the atomic scale within the millisecond regime.^{52,53} In combination with the network detection software, tracing structural dynamic changes and transitions in network structures becomes possible.

At the macroscopic scale, the evolution and the growth of structural arrangements could be monitored. Studies of macroscopic samples could be based on conventional videos or photo

series. We are convinced that students and researchers from different disciplines will identify a wide variety of possible applications to study networks at different length scales with our program. These hands-on analyses can extend beyond the typical textbook examples of ordered structures.

SUPPLEMENTAL MATERIAL

See the supplementary material for additional examples of honeycomb-like structures that have been analyzed with our Python software. For the ease of use, we provide an introductory video how to operate our Python network detection program. The video shows how to perform network analysis using honeycombs as example, including the following steps: (1) image import, (2) feature class creation, (3) ring center detection, (4) interactive correction of auto-detection, (5) network creation, and (6) file export.

ACKNOWLEDGMENTS

The authors thank Wolf-Dieter Schneider fruitful discussions. This project has received funding from the European Research Council (ERC) under the European Unions Horizon 2020 Research and Innovation Program (Grant Agreement No. 669179). LG acknowledges support by the IMPRS for Elementary Processes in Physical Chemistry.

AUTHOR DECLARATIONS

Conflict of Interest

The authors have no conflicts to disclose.

Author Contributions

Leonard Gura: Conceptualization (equal); Data curation (equal); Formal analysis (equal); Investigation (equal); Software (equal); Visualization (equal); Writing – original draft (equal). **Matthias Brinker:** Data curation (equal); Investigation (equal); Software (equal); Visualization (equal). **Patrik Marschalik:** Investigation (equal); Software (equal); Visualization (equal). **Florian Kalaf:** Data curation (equal); Investigation (equal); Software (equal); Visualization (equal). **Bettina Junkes:** Data curation (equal); Resources (equal). **Heinz Junkes:** Software (equal); Visualization (equal). **Markus Heyde:** Conceptualization (equal); Methodology (equal); Project administration (equal); Supervision (equal); Validation (equal); Writing – review & editing (equal). **Hans-Joachim Freund:** Funding acquisition (equal); Resources (equal); Writing – review & editing (equal).

DATA AVAILABILITY

The data that support the findings of this study are available from the corresponding author upon reasonable request.

REFERENCES

- ¹W. C. Graustein, *Ann. Math.* **32**, 149 (1931), <http://www.jstor.org/stable/1968421>.
- ²E. B. Matzke, *Am. J. Bot.* **33**, 58 (1946), see <http://www.jstor.org/stable/2437492>.

- ³W. Borchardt-Ott, *Crystallography: An Introduction* (Springer Science & Business Media, 2011).
- ⁴K. Hermann, *Crystallography and Surface Structure: An Introduction for Surface Scientists and Nanoscientists* (John Wiley & Sons, 2016).
- ⁵J. Couzin, *Science* **309**, 83 (2005).
- ⁶W. H. Zachariasen, *J. Am. Chem. Soc.* **54**, 3841 (1932).
- ⁷M. A. Springer, T.-J. Liu, A. Kuc, and T. Heine, *Chem. Soc. Rev.* **49**, 2007 (2020).
- ⁸Y. Iqbal, H. O. Jeschke, J. Reuther, R. Valentí, I. I. Mazin, M. Greiter, and R. Thomale, *Phys. Rev. B* **92**, 220404 (2015).
- ⁹Y. Jing and T. Heine, *Nat. Mater.* **19**, 823 (2020).
- ¹⁰Y.-X. Jiang, J.-X. Yin, M. M. Denner, N. Shumiya, B. R. Ortiz, G. Xu, Z. Guguchia, J. He, M. S. Hossain, X. Liu *et al.*, *Nat. Mater.* **20**, 1353 (2021).
- ¹¹H. P. Boehm., A. Clauss, G. O. Fischer, and U. Hofmann, *Z. Naturforsch. B* **17**, 150 (1962).
- ¹²H. P. Boehm, A. Clauss, G. O. Fischer, and U. Hofmann, *Z. Anorg. Allg. Chem.* **316**, 119 (1962).
- ¹³H.-P. Boehm, *Angew. Chem. Int. Ed.* **49**, 9332 (2010).
- ¹⁴K. S. Novoselov, A. K. Geim, S. V. Morozov, D. Jiang, Y. Zhang, S. V. Dubonos, I. V. Grigorieva, and A. A. Firsov, *Science* **306**, 666 (2004).
- ¹⁵K. S. Novoselov, A. K. Geim, S. V. Morozov, D. Jiang, M. I. Katsnelson, I. V. Grigorieva, S. V. Dubonos, and A. A. Firsov, *Nature* **438**, 197 (2005). ISSN 1476-4687.
- ¹⁶P. J. M. Swinkels, Z. Gong, S. Sacanna, E. G. Noya, and P. Schall, *Nat. Commun.* **14**, 1524 (2023).
- ¹⁷G. Binnig, H. Rohrer, C. Gerber, and E. Weibel, *Phys. Rev. Lett.* **49**, 57 (1982).
- ¹⁸R. Wiesendanger, *Scanning Probe Microscopy and Spectroscopy: Methods and Applications* (Cambridge University Press, Cambridge, 1994), see <https://www.cambridge.org/core/books/scanning-probe-microscopy-and-spectroscopy/92B4C6E961A09D23635AF7A3DC62FC42>.
- ¹⁹L. Lichtenstein, C. Büchner, B. Yang, S. Shaikhutdinov, M. Heyde, M. Sierka, R. Włodarczyk, J. Sauer, and H.-J. Freund, *Angew. Chem. Int. Ed.* **51**, 404 (2012).
- ²⁰L. Lichtenstein, M. Heyde, and H.-J. Freund, *J. Phys. Chem. C* **116**, 20426 (2012).
- ²¹Y. Li and D. A. Drabold, *Phys. Stat. Sol. (b)* **250**, 1012 (2013).
- ²²M. O. Blunt, J. C. Russell, N. R. Champness, and P. H. Beton, *Chem. Commun.* **46**, 7157 (2010).
- ²³P. Y. Huang, S. Kurasch, J. S. Alden, A. Shekhawat, A. A. Alemi, P. L. McEuen, J. P. Sethna, U. Kaiser, and D. A. Muller, *Science* **342**, 224 (2013).
- ²⁴J.-Q. Zhong and H.-J. Freund, *Chem. Rev.* **122**, 11172 (2022).
- ²⁵A. L. Lewandowski, S. Tosoni, L. Gura, Z. Yang, A. Fuhrich, M. J. Prieto, T. Schmidt, D. Usvyat, W.-D. Schneider, M. Heyde, G. Pacchioni, and H.-J. Freund, *Chemistry* **27**, 1870 (2021).
- ²⁶M. Pivetta, M.-C. Blüm, F. Pathney, and W.-D. Schneider, *Angew. Chem. Int. Ed.* **47**, 1076 (2008).
- ²⁷L. Sir Bragg and J. F. Nye, *Naturwissenschaften* **34**, 328 (1947).
- ²⁸K. M. Burson, P. Schlexer, C. Büchner, L. Lichtenstein, M. Heyde, and H.-J. Freund, *J. Chem. Educ.* **92**, 1896 (2015).
- ²⁹P. Thomison, *Troubleshooting Abnormal Corn Ears* (2023), see <https://u.osu.edu/mastercorn/>.
- ³⁰M. A. Wilson, *Favosites from the Upper Ordovician of southern Indiana, USA* (2010), see <https://en.wikipedia.org/wiki/Favosites>.
- ³¹C. W. W. Pirk, H. R. Hepburn, S. E. Radloff, and J. Tautz, *Naturwissenschaften* **91**, 350 (2004).
- ³²D. Bauer and K. Bienefeld, *Naturwissenschaften* **100**, 45 (2013).
- ³³B. L. Karihaloo, K. Zhang, and J. Wang, *J. R. Soc. Interface* **10**, 20130299 (2013).
- ³⁴R. Oeder and D. Schwabe, *Apidologie* **52**, 174 (2021).
- ³⁵C. Darwin, *The Origin of Species by Means of Natural Selection* (Pub One Info, 1859).
- ³⁶J. Wyman, *Notes on the Cells of the Bee* (Cambridge: Welch, Bigelow, and Company, 1866).
- ³⁷G. Van Rossum and F. L. Drake, *Python 3 Reference Manual* (CreateSpace, Scotts Valley, CA, 2009). ISBN: 1441412697.
- ³⁸M. B. Leonard Gura, *Visualyse, GitHub repository*, see <https://github.com/molgen.mpg.de/gura/Visualyse> (2022), <https://www.hvg-dgg-events.com/iyog2022-germany>.

- ³⁹M. Maraldi, *Mem. Acad. R. Sci.* **T31**, 381 (1712).
- ⁴⁰C. D. Michener, *The Bees of the World* (The Johns Hopkins University Press, 2000).
- ⁴¹F. Atamny, O. Spillecke, and R. Schlögl, *Phys. Chem. Chem. Phys.* **1**, 4113 (1999).
- ⁴²K. M. Burson, C. Büchner, M. Heyde, and H.-J. Freund, *J. Phys.: Condens. Matter* **29**, 035002 (2017).
- ⁴³K. M. Burson, H. J. Yang, D. S. Wall, T. Marsh, Z. Yang, D. Kuhness, M. Brinker, L. Gura, M. Heyde, W.-D. Schneider, and H.-J. Freund, *J. Phys. Chem. C* **126**, 3736 (2022).
- ⁴⁴T. Fukuma, K. Kobayashi, K. Matsushige, and H. Yamada, *Appl. Phys. Lett.* **87**, 034101 (2005).
- ⁴⁵W. Schroeder, K. Martin, and B. Lorenzen, *The Visualization Toolkit* (2006), 4th ed., ISBN: 978-1-930934-19-1.
- ⁴⁶L. Grady, *IEEE Trans. Pattern Anal. Mach. Intell.* **28**, 1768 (2006). ISSN 1939-3539.
- ⁴⁷E. Gouillart, *A tutorial on segmentation*, see <https://emmanuelle.github.io/a-tutorial-on-segmentation.html> (2015), <https://emmanuelle.github.io/a-tutorial-on-segmentation.html>.
- ⁴⁸A. Stone and D. Wales, *Chem. Phys. Lett.* **128**, 501 (1986).
- ⁴⁹G. J. Dienes, *J. Appl. Phys.* **23**, 1194 (1952).
- ⁵⁰A. Hagberg, P. Swart, and D. S. Chult (2008), see <https://www.osti.gov/biblio/960616>.
- ⁵¹L. Gura, S. Tosoni, A. L. Lewandowski, P. Marschalik, Z. Yang, W.-D. Schneider, M. Heyde, G. Pacchioni, and H.-J. Freund, *Phys. Rev. Mater.* **5**, L071001 (2021).
- ⁵²L. Gura, Z. Yang, M. Brinker, F. Kalaf, W. Kirstaedter, P. Marschalik, H. Junkes, M. Heyde, and H.-J. Freund, *Appl. Phys. Lett.* **119**, 251601 (2021).
- ⁵³Z. Yang, L. Gura, F. Kalaf, P. Marschalik, M. Brinker, W. Kirstaedter, J. Hartmann, G. Thielsch, H. Junkes, M. Heyde, and H.-J. Freund, *Rev. Sci. Instrum.* **93**, 053704 (2022).